Journal of Molecular Structure 1352 (2026) 144569

Contents lists available at ScienceDirect

Journal of Molecular Structure

journal homepage: www.elsevier.com/locate/molstr

Biosynthesis, characterization, antimicrobial and adsorbent effects of γ-aluminum oxide-NPs using aqueous extract of boswellia carterii resin

Waleed Khalid Mahdi [a,*], Aqeel Oudah Flayyh [b], Falih Hassan Musa [c], Ahmed Saleem Otaiwi [d]

[a] Department of Chemistry, College of Education of Pure Science, Ibn Al-Haitham, University of Baghdad, Baghdad, Iraq
[b] Al-Husseinya secondary evening school for boys, Ministry of Education, Baghdad, Iraq
[c] Deen of College of Health and Medical Technology / Ashur University, Baghdad, Iraq
[d] Researcher Chemist, Ministry of Water Resources. Baghdad, Iraq

ARTICLE INFO

Keywords:
Green synthesis
Γ-Al_2O_3-NPs spectroscopy
Antibacterial activity
Male frankincense resin
Adsorbent

ABSTRACT

γ-Al_2O_3—NPs were synthesized by a green synthesis process based on *Boswellia carterii* resin extract and aluminum sulphate in an alkaline medium. *Boswellia carterii* resin extract is a significant reducing and stabilizing agent for synthesizing γ-Al_2O_3—NPs.Several techniques, including Fourier–transform infrared (FT-IR), UV–visible spectroscopy, x-ray diffraction, electron microscopy (XRD), energy dispersive x-ray (EDX), scanning electron microscopy (SEM), Transmission electron microscopy (TEM), and atomic force microscopy (AFM), were utilized to investigate the final product. XRD and SEM confirmed a plate-like crystalline structure with an average size of 17.5 nm. FT-IR analysis identified aluminum oxide stretching vibrations (655, 451) cm^{-1}, U.V.-visible spectroscopy exhibits an absorption band at 252 nm, and the energy gap, Eg, of 4.91 eV. EDX confirmed the presence of Al, and O TEM and AFM showed agglomerated spherical plates. Antimicrobial assay revealed the highest inhibition at 0.25mg/mL with a decrease in concentration from 2mg/mL to 0.25mg/mL for *Staphylococcus aureus, Escherichia coli*, and *Candida albicans* fungi. Adsorption studies by U.V-visible spectroscopy demonstrated high metal ion (II) removal efficiencies: Co (89.18 %), Ni (87.33 %), and Cu (90.42 %).

1. Introduction

Enhancing the environmentally friendly and sustainable pathways for producing nanoparticles (NPs) is an essential component of green nanotechnology [1]. Successful methods have been used in green chemistry for the synthesis of aluminum oxide nanoparticles, so these methods are effective in terms of reducing environmental pollution. Hazardous, costly, time-consuming, and hazardous to both people and the environment [2–7].

Green synthesis methods present a feasible option through which biobased materials, like microorganisms, plants, and agricultural waste, can serve as environmentally benign sources for nanoparticle synthesis [8,9].

Nano- Aluminum oxide (N-AlO) has desirable properties: chemical stability, high melting temperature, strong electrical insulation, low thermal conductivity, superior corrosion resistance, high strength to density ratio, and light weight [10]. Al_2O_3 NPs, employed in many fields such as ceramics and the textile industries [11,12] .

Recently, there has been an interest in preparing Al_2O_3 Nps and selecting them as suitable for antibacterial inhibition, and capacity for removing metal ions from aqueous solution by adsorption media. This study thoroughly evaluated the primary techniques for the synthesis and functionalization of nanoparticles, clarified the fundamental mechanisms that drive their antibacterial properties against both Gram-negative and Gram-positive bacteria, and analyzed the impact of morphological variations on their antibacterial efficacy [13].

Nano-structured γ-Al_2O_3NPs synthesized by the Arc Discharge method showed potent antibacterial activity against drug-resistant Acinetobacter baumanii, with an inhibition zone diameter of 19 mm [14]. Musa F.H.et al. prepared γ-Al_2O_3NPs by using aqueous clove extract. The size range of nanoparticles was (28- 37) nm. Antimicrobial activity showed inhibition activity of γ-Al_2O_3NPs against *Escherichia coli* negative (G^-), *Staphylococcus aureus*, positive (G^+), and *Candida albicans* fungal with concentration (2–0.25) mg / mL in the range (31- 15) mm.

* Corresponding author.
E-mail addresses: waleed.k.m@ihcoedu.uobaghdad.edu.iq (W.K. Mahdi), oqil.awda1205a@ihcoedu.uobaghdad.edu.iq (A.O. Flayyh), falih.hassan@au.edu.iq (F.H. Musa), ahmedrawe@hotmail.com (A.S. Otaiwi).

https://doi.org/10.1016/j.molstruc.2025.144569
Received 26 June 2025; Received in revised form 6 September 2025; Accepted 27 October 2025
Available online 29 October 2025

γ-Al_2O_3NPs used as absorbent on binary metal ions: Co, Ni, Cu, by removing them from water with efficient absorbance. 93.22 %, 87.49 %, and 93.17 % respectively [15].

Another study, γ-Al_2O_3NPs were prepared using aqueous cinnamon extract with a particle size of 62.71 nm. The efficiency of the Al_2O_3NPs was examined for resistance to the bacteria *E. coli, Staphylococcus aureus*, and *Candida albicans* with a concentration of 2–0.25 mg/mL. The efficient inhibition (17 – 27) mm. Al_2O_3NPs used as an adsorbent to remove binary metal cations, Ni, Co, Cu, from aqueous solution. The percentage of these ions that were removed was 84.42 %, 91.25 % and 93.81 % respectively [16]. The study aims to prepare γ-Al_2O_3NPs by using aqueous extract of Boswellia Carterii – Resin, for the potential application as antibacterial activity and good removal of ions from aqueous solution based on a low–cost, simple, and reliable method.

2. Experimental section

2.1. Materials

The chemicals used in this study are aluminum sulphate, $Al_2(SO_4)_3$ (Germany/Merck), NaOH from (India/ Alpha chemicals), Absolute ethanol (RBL/Spain), cobalt (II) sulphate, $CoSO_4$, copper (II) sulphate pentahydrate, $CuSO_4{\cdot}5H_2O$, and nickel (II) sulphate heptahydrate, $NiSO_4{\cdot}7H_2O$. *Boswellia Carterii* resin was taken from the local Baghdad market, where it is collected.

2.2. Instrumentation

Electronic Balance (A220/C/1 model), PLC Centrifuge (4000–4500 rpm), (FAITHFUL) Electric oven, water bath with shaking (SCL F), Tape of pH, spectrum of (160/UV) Shimadzu spectroscopy. The studies of FTIR have been recorded by using (8500S) type Shimadzu in the range (400–4000cm^{-1}) from Baghdad University, and (XRD) (Holland/Phillips) in the laboratory center of Baghdad. (SEM) type (300 Hv/Germany-Z.S), (EDX), (TEM) type (100Kv / Germany), at (Kashan University /Iran). A (AFM), type (Nano surf AG. Liestal), Switzerland, was conducted at the College of Science /University of Baghdad. The Synthetic γ-Al_2O_3NPs were tested against two reference bacteria, *Staphylococcus aureus* (G^+), *E. coli* (G^-), and the fungal *Candida albicans*, by diffusion method and nutrient medium, type Mueller Hinton agar (MHA), and Potato Dextrose Agar (PDA).

2.3. Preparation of the plant extract

In the biosynthesis process, initially, to prepare the extract, 20 g of *Boswellia carterii* (male frankincense) resin is taken from the bark of the tree, washed well with water to get rid of any contaminants, and then left to dry at the lab temperature. After that, a 500 mL beaker is filled with the pulverized plant resin, then 200 mL of deionized water is added to it, and mixed well through continuous stirring for 30 min to obtain a milky-colored extract solution, then left to cool at room temperature and then filtered using Whatman filter paper (No.1). After that, the resulting solution is separated by using a centrifuge at 4000 rpm for a quarter of an hour. After that, the product containing the extract solution of Boswellia resin is collected in a round flask.

2.4. Synthesis and characterization of γ-Al_2O_3–NPs

In 30 mL of deionized water, 3.75 g of $Al_2(SO_4)_3$ was dissolved, followed by the addition of 100 mL of *Boswellia carterii* resin extract under continuous stirring. As the temperature decreased, a 1 M NaOH solution was gradually added while monitoring the color change of the mixture

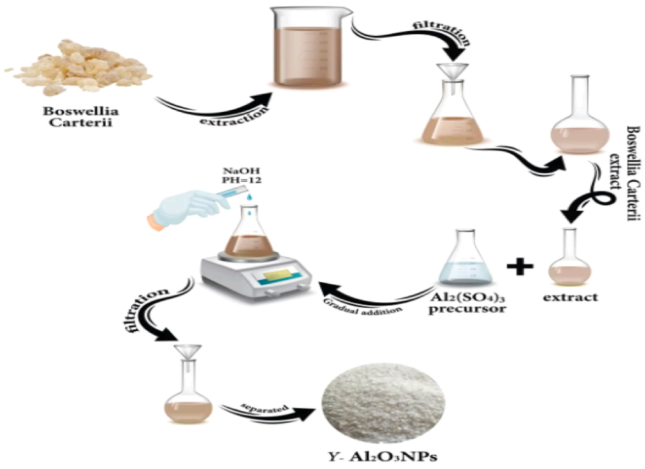

Fig. 1. The preparation steps of γ-Al_2O_3–NPs powder using Boswellia carterii resin extract.

Fig. 2. Colour change of solutions of $Al_2(SO_4)_3$ and bio–redactor of Boswellia carterii resin extract **(a)** dark Peggy, **(b)** Milky, **(c)** Pale Peggy, and **(d)** γ-Al_2O_3–NPs powder.

until the pH reached 12.0. The product was then allowed to stand for 48 h to precipitate, forming a creamy precipitate, which was separated by centrifugation and dried in an electric oven at 300 °C for 10 h. This process yielded a white powder of γ-Al_2O_3 nanoparticles. The synthesis procedure of alumina nanoparticle powder using the aqueous extract of *Boswellia carterii* resin is illustrated in Fig. 1.

2.5. Antimicrobial method

In this work, the pathogenic bacterial strains are *E. coli* (G-) bacteria, *Staphylococcus aureus* (G^+) bacteria, and *Candida albicans*. The diffusion approach was used for evaluating γ-Al_2O_3NPs' antibacterial activity. γ-Al_2O_3. Petri dishes were sterilized and used in addition to Luria Broth Agar (LBA), where individual bacterial isolates were grown in an incubator for 24 h and spread separately on an agar medium. A cork was

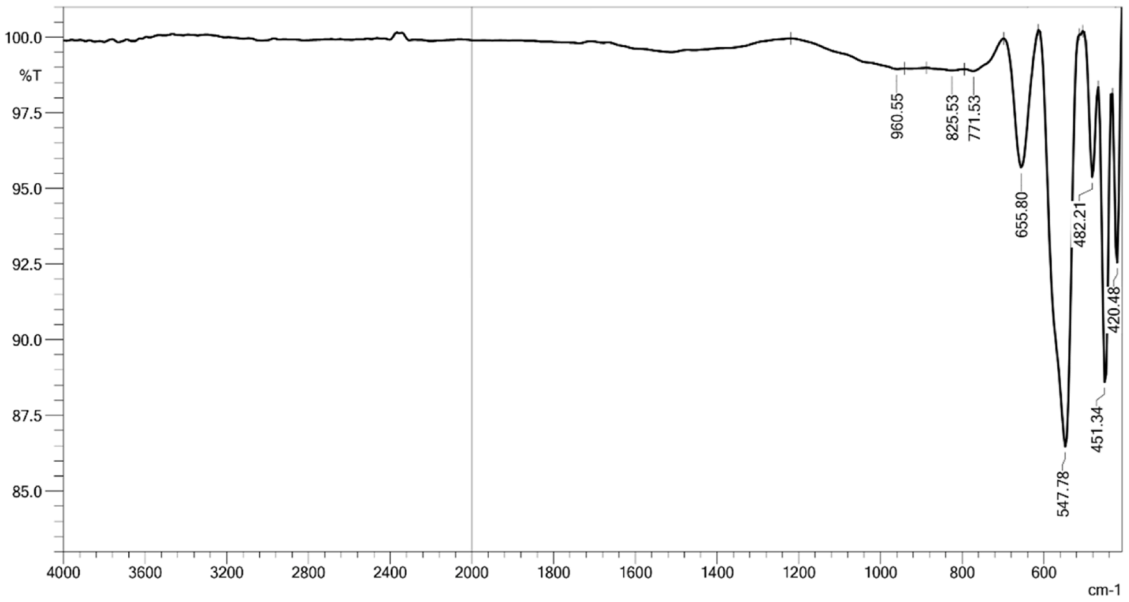

Fig. 3. FTIR spectrum for γ-Al_2O_3–NPs powder.

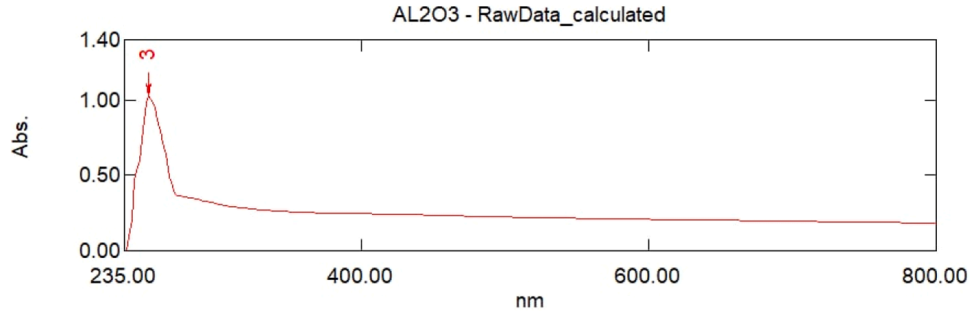

Fig. 4. UV–vis absorption spectrum of γ-Al_2O_3–NPs powder.

drilled to create a well with a diameter of 6 mm, making sure that it was under sterile conditions.

The propagation method was used on fungi of type *Candida albicans* in the presence of a tablet with a nutrient medium of type (MHA), and its antifungal activity was assessed using the same technique. Potato was used as a mediator for nutrients agar of type (PDA) dextrose with different concentrations of γ-Al_2O_3–NPs, which are 0.25mg/mL, 0.5mg/mL, 1 mg/mL, and 2 mg/mL.

In this case, sterile water is used to disperse γ-Al_2O_3–NPs, and fine sterile pipettes are added to the wells. The plates were incubated at 37 °C for 36 hr., and then the inhibition zone values for each well were recorded. The values were noted, and then, for the ultimate antibacterial activity, these values were computed in mm.

2.6. Adsorption method

While applying this method, I used a variable ionic metal solution with a concentration of 0.00005 g/mL prepared by optimal dilution of stock solution with stirring for 30 min at pH= 6, and in the end, it was filtered and then filtrated, after which the effect of changing the concentration of metal ions cobalt, nickel, and copper from 1–10 mg/L with 0.5 g of adsorbents was studied at the contact time, which is 30 min.

3. Results and discussion

An aqueous extract of *Boswellia carterii* resin was used with $Al_2(SO_4)_3$. The changing colour solutions are shown in (Fig. 2a) from dark Peggy to Milky in (Fig. 2b), and after that to Pale Peggy in (Fig. 2c), and also a white powder of γ-Al2O3-NPs as shown in (Fig. 2d).

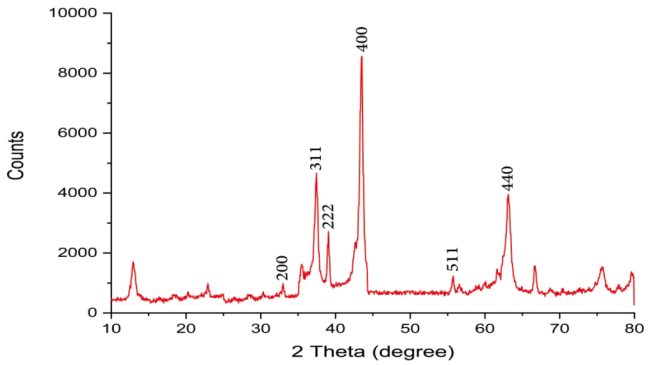

Fig. 5. XRD pattern of γ-Al_2O_3–NPs powder.

3.1. FT-IR spectroscopic study

FT-IR spectrum of the Al_2O_3NPs is shown in Fig. 3, with a very weak broadband exhibited at 3400 cm^{-1} due to O—H bands and band vibration of C—H bond located at 2300 cm^{-1}. Bands in the range 566 cm^{-1} to 451 cm^{-1}, attributed to the Al-O of bending vibration for Al–OH groups [16,17].

Table 1
XRD analysis results of γ-Al_2O_3—NPs.

2-Theta	hkI	FWHM	Xs(nm)	Average Crystallite Size (nm)
33.395	200	0.412	20.58	17.5
36.501	311	0.57	15.33	
39.89	222	0.58	15.23	
44.161	400	0.407	22.01	
56.505	511	0.473	19.92	
63.937	440	0.82	11.93	

The Al-O stretching vibration was represented by the band at 655 cm^{-1} [18]. The peak at 771cm-1, which is due to the Al-O-Al stretching frequency for octahedral coordinated aluminum, also showed alumina crystallization [19].

3.2. Studies and evaluation of (UV–vis) spectroscopic and band gap energy

The electronic spectrum of Al_2O_3—NPs displayed a peak at λ_{max} = 252 nm in the UV region Fig. 4 [16]. The equation calculated the energy band gap (Eg): E_g (eV) = 1239.83 / λ (nm), where λ is wavelength, E_g is the energy gap, Eg =1239.83/252 = 4.91 eV [20,21].

3.3. XRD analysis

For the phase formation and crystallite size, as shown in paragraph Fig. 5, diffraction peaks can be associated with 2θ: 33.39°, 36.50°, 39.89°, 44.16°, 56.50°, and 63.93°, with index Miller of (200), (311), (222), (400), (511), and (440) respectively.

The reflection and broadening indicate the nano crystals' inherent nature. The calculated crystalline size was from (FWHM). Diffraction peaks and (β) were used from the method of Debye – Scherer, using the simple equation of $d = K\lambda / \beta\cos\theta$, where d refers to the average crystalline dimension perpendicular to the reflective phases, β is the full width at half maximum (FWHM), K is Scherer's constant 0.92, λ is the x-ray wavelength, θ is the Bragg's angle [22,23]. The Bragg reflection intensity without the use of an instrument for broadening, and the average crystallite size of the products was determined to be 17.5 nm. The obtained diffraction exhibited the nature of the crystalline sample with the pure rhombohedral structure phase of γ-Al_2O_3NPs matched with reference pattern JCPDS card No: 00–029–0063, as shown in Table 1 [24]. The calculation of crystallinity index is by using Eq. (1) below:

$$I_{cry} = \frac{D_p(TEM)}{D_{cry}(XRD)} \quad (1)$$

Where I_{cry} is the crystallinity index; D_p is the particle size (TEM), and D_{cry} is the particle size (Scherrer equation). The I_{cry} index was higher than 1.0, illustrating that γ-Al_2O_3NPs were polycrystalline [14].

3.4. Morphological analysis

The SEM and TEM images (Fig. 6A and 6B) showed that the morphology and size of the synthesized Al_2O_3—NPs are irregularly spherical and uniform in size with a plate-like distribution. The average particle size is 17.5 nm [25,26].

3.5. EDX analysis

The EDX results for Al_2O_3—NPs, Fig. 7, sho**wed no impurities, revealing the presence of** aluminum and oxygen. This proves that alumina is chemically pure [27].

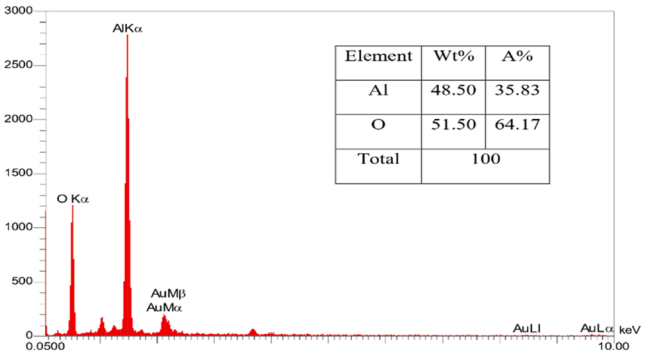

Fig. 7. EDX of γ-Al_2O_3—NPs powder.

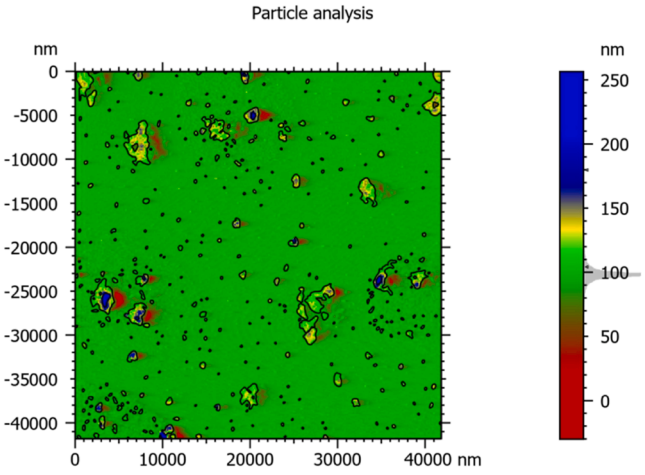

Fig. 8. AFM particle analysis and threshold detection of γ-Al_2O_3NPs powder.

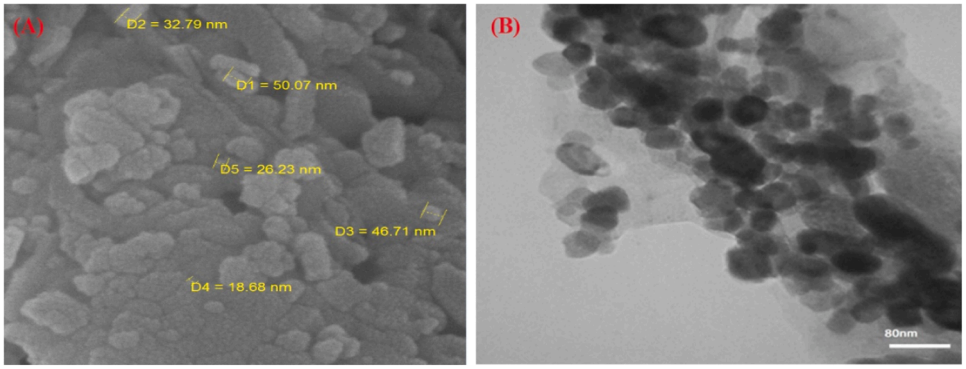

Fig. 6. (A) SEM and **(B)** TEM images of γ-Al_2O_3—NPs powder.

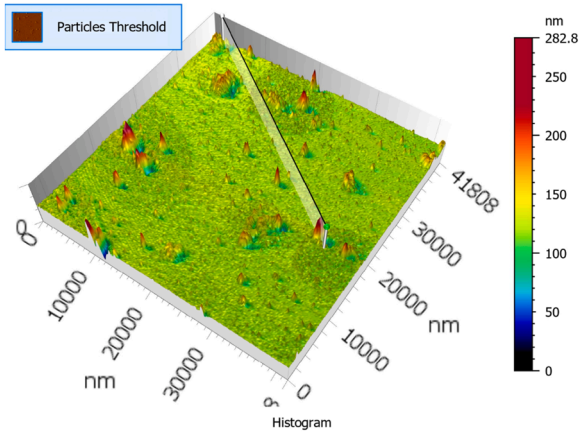

Fig. 9. AFM image of particle threshold of γ-Al_2O_3—NPs powder.

Table 2
AFM information and individual results with global statistics of γ-Al_2O_3—NPs powder.

Individual Results				
Particle	Projected Area	Projected area (nm^2)	Mean diameter (nm)	Z-maximum (nm)
Particle #1	Large	26,881	93.29	105
Particle #2	Large	26,881	93.29	105
Particle #3	Large	26,881	93.29	105
Particle #4	Large	26,881	93.29	105
Particle #5	Large	26,881	93.29	105
Particle #6	Large	26,881	93.29	105
Global Statistics				
Metric	Projected area (nm^2)	Mean diameter (nm)		Z-maximum (nm)
Mean	64,247	134.9		111.2
Min	7560	60.75		105
Max	7948,858	3073		223.5
Information				
Parameter		Value		
Threshold 1		105.0 nm		
Number of particles		2134		

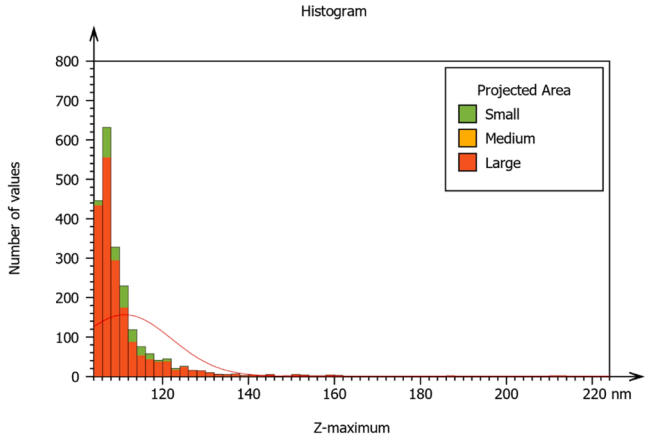

Fig. 10. AFM histogram and statistical particle analysis of γ-Al_2O_3—NPs powder.

3.6. AFM analysis

This AFM technique was used to investigate the aggregation and dispersion of nanomaterials, in addition to their shape, size, structure, and sorption (Figs. 8 and 9), and Table 2 showed particle analysis—threshold detection and the information with individual results and global statistics of γ-Al_2O_3—NPs powder [28,29].

The AFM histogram and statistical particle analysis of γ-Al_2O_3—NPs are shown in Fig. 10 [15] .Length, width, height particle analysis are shown in Figs. 11 and 12, and the topography parameters of other particle analysis are shown in Figs. 13a, 13b, 14a, 14b, and 15 [30,31].

3.7. Antimicrobial study

The antibacterial inhibition of Al_2O_3NPs was previously tested against several pathogens [14,32–35].

The antibacterial properties of γ-Al_2O_3NPs in diluted HCl were evaluated against *E. coli, Staphylococcus aureus,* and *Candida albicans* fungi using the diffusion method. Through these obtained results, it was found that HCl dilution did not show any inhibition zone, according to the antibacterial negative and positive anti.

The results are presented in Table 3, showing a higher antibacterial activity occurring with a decrease in concentration from 2 mg/mL, 1 mg/mL, 0.5 mg/mL, and 0.25 mg/mL, and also an increase in the Candida albicans activity occurring with decreasing concentration from 2 mg/mL to 0.25 mg/mL [36].

The main mechanism suggested that the electrostatic interaction of Al_2O_3NPs with the bacterial outer membrane/cell wall and formation of Al^{+3} can enable the bacteriostatic effect of these nanoparticles, and that will initiate a reactive oxygen species (ROS) increment and oxidize the cell wall [13].

The WHO's 2024 Bacterial Priority Pathogens List highlights critical and high-priority antibiotic-resistant bacteria to guide research and public health interventions effectively. Scientific studies have demonstrated their significant antibacterial properties against various bacterial strains, including multidrug-resistant clinical isolates. Aluminum oxide nanoparticles exhibit bacteriostatic and bactericidal effects, largely through mechanisms such as electrostatic interaction with bacterial membranes and induction of oxidative stress via reactive oxygen species (ROS) generation. Their effectiveness has been shown against both Gram-negative and Gram-positive bacteria, with inhibitory concentrations varying by strain but generally demonstrated at concentrations of 1000 μg/mL or higher [37].

3.8. Adsorption study

Several analytical methods have been developed to remove trace amounts of heavy metal ions from industrial wastewater, such as adsorption, chemical precipitation, , ion flotation, and electrochemical ion exchange, and these approaches can effectively remove heavy metals from water [38].

Most of the time, these methods are complex and cost a lot. Alternative methods, using adsorbents, like resin, nanometal oxide, have been studied to remove Cd (II) from outlet water [39,40].

Dodonaea angustifolia extract-assisted green synthesis of Cu_2O / Al_2O_3 nanocomposite for the adsorption of Cd (II) from water achieved by Girma M. W et al.

The Cu_2O/Al_2O_3 nanocomposite adsorbed rapidly, and after 60 min, it attained adsorption equilibrium, removing 97.36 % of Cd (II) from the water. In connection with our previous research [9].

γ-Al_2O_3—NPs were obtained by using aqueous extract of Boswellia carterii resin, used as an adsorbent for metal cations from aqueous solution. considering Fig. 16, the data clarified the rate of adsorption of metal bivalent cations. Co, Ni, and Cu from aqueous solution were 89.42 %, 90.90 %, and 86.92 % respectively. The results indicate that the effectiveness of metal ion removal increased with 10 min.

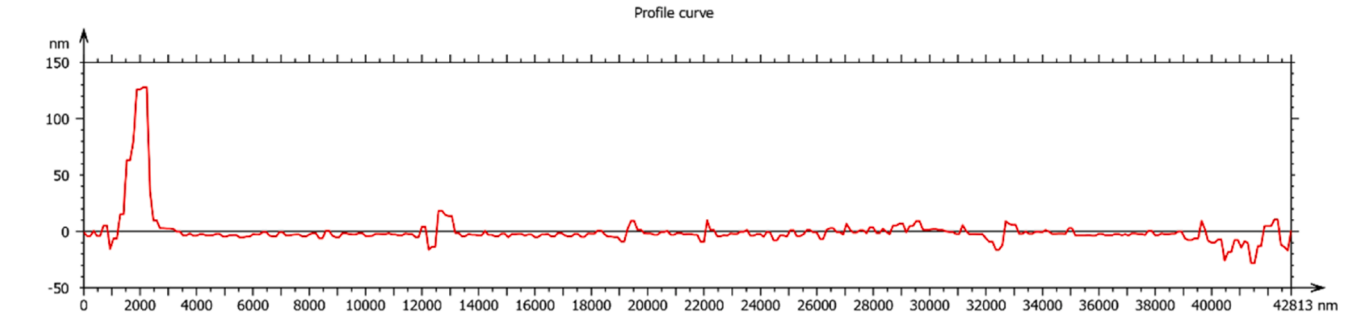

Parameters	Value	Unit
Length	42813	nm
Shown scale	200.0	nm

Fig. 11. AFM curve of particle analysis length of γ-Al_2O_3–NPs powder.

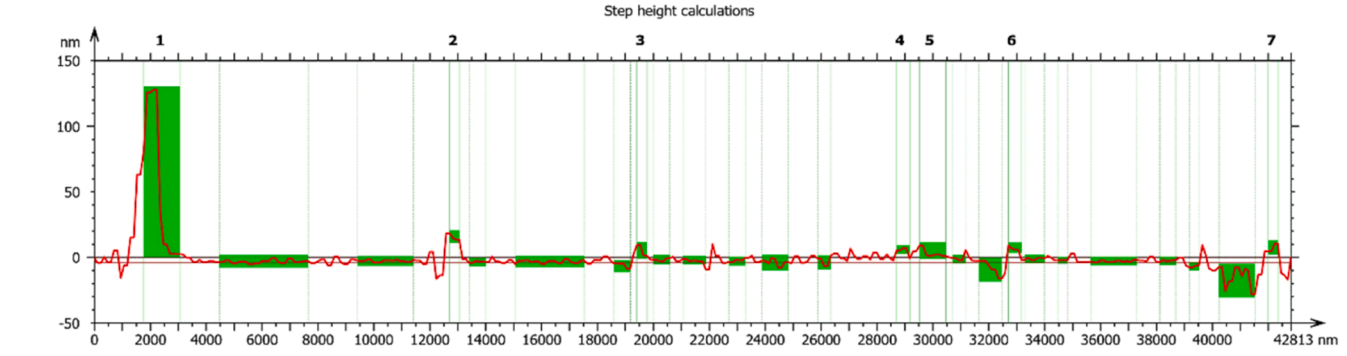

Parameters	Unit	Mean	Min	Max	Step 1	Step 2	Step 3	Step 4	Step 5	Step 6	Step 7
Width	nm	604.9	352.9	1294	1294	352.9	352.9	470.5	941.0	470.5	352.9
Maximum height	nm	31.28	10.95	131.8	131.8	22.33	13.33	10.95	13.06	12.97	14.47
Mean height	nm	18.92	7.488	63.15	63.15	19.54	10.72	10.07	7.488	10.89	10.60

MountainsSPIP® Academic 9.2.9994

Fig. 12. AFM height and width calculations parameters of γ-Al_2O_3–NPs powder.

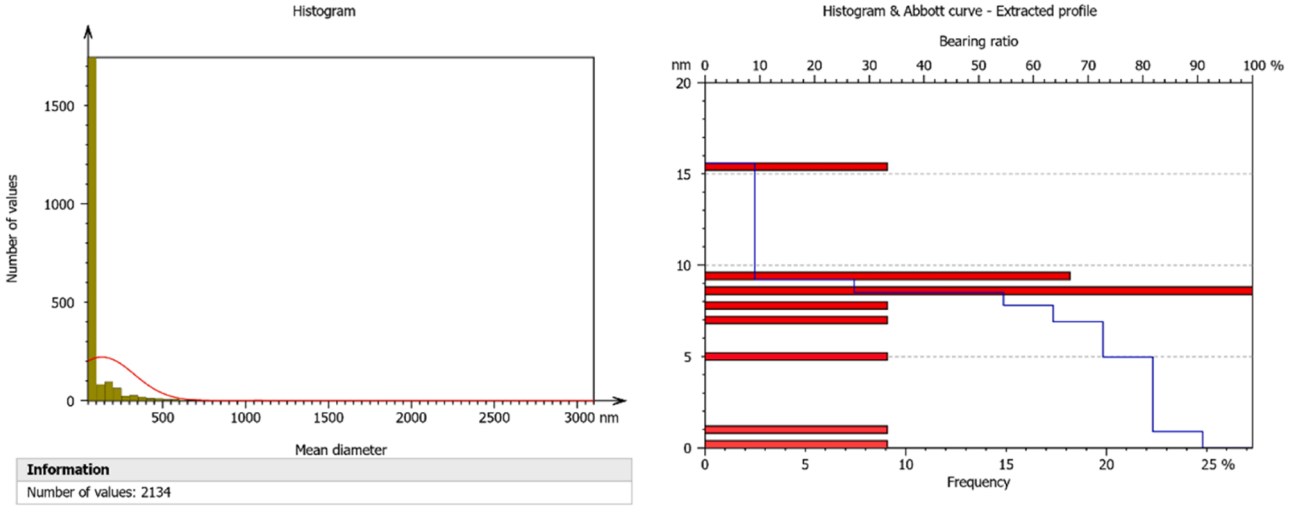

Information
Number of values: 2134

Fig. 13. AFM **(a)** histogram Number of values against mean diameter, **(b)** Abbott curve – extracted profile explains the bearing ratio against the frequency of γ-Al_2O_3–NPs powder.

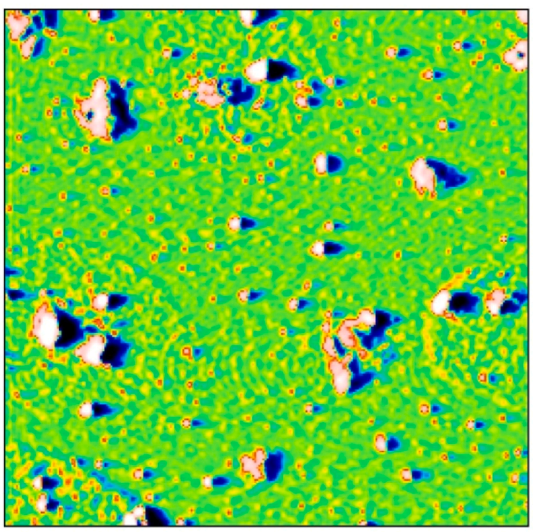

ISO 25178 - Roughness (S-L)			
F: [Workflow] Form removed (LS-poly 3)			
S-filter (λs): Gaussian, 0.8 µm			
L-filter (λc): Robust Gaussian (order 1), 0.0025 mm			
Height parameters			
Sq	8.438	nm	*Root-mean-square height*
Ssk	2.115		*Skewness*
Sku	52.33		*Kurtosis*
Sp	129.0	nm	*Maximum peak height*
Sv	102.2	nm	*Maximum pit depth*
Sz	231.2	nm	*Maximum height*
Sa	3.001	nm	*Arithmetic mean height*
Functional parameters			
Smr	100.0	%	*Areal material ratio*
Smc	2.388	nm	*Inverse areal material ratio*
Sdc	4.992	nm	*Material ratio height difference*
Hybrid parameters			
Sdq	0.0266		*Root-mean-square gradient*
Sdr	0.03507	%	*Developed interfacial area ratio*

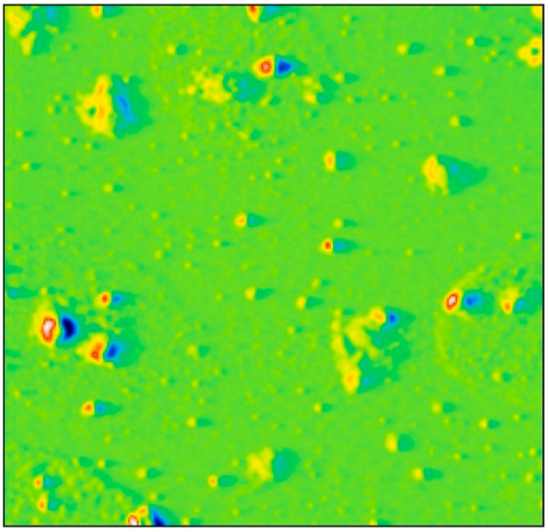

ISO 25178 - Primary surface			
F: [Workflow] Form removed (LS-poly 3)			
F: Leveled (LS), Angle 2.28e-11°, 2.872e-11°			
S-filter (λs): Gaussian, 0.8 µm			
Height parameters			
Sq	8.789	nm	*Root-mean-square height*
Ssk	1.630		*Skewness*
Sku	47.06		*Kurtosis*
Sp	130.5	nm	*Maximum peak height*
Sv	107.6	nm	*Maximum pit depth*
Sz	238.1	nm	*Maximum height*
Sa	3.334	nm	*Arithmetic mean height*
Functional parameters			
Smr	100.0	%	*Areal material ratio*
Smc	2.856	nm	*Inverse areal material ratio*
Sdc	6.055	nm	*Material ratio height difference*
Hybrid parameters			
Sdq	0.02673		*Root-mean-square gradient*
Sdr	0.03541	%	*Developed interfacial area ratio*

(a) **(b)**

Fig. 14. AFM images: **(a)** Roughness (S-L), **(b)** Primary surface, and their topography parameters of γ-Al_2O_3–NPs powder.

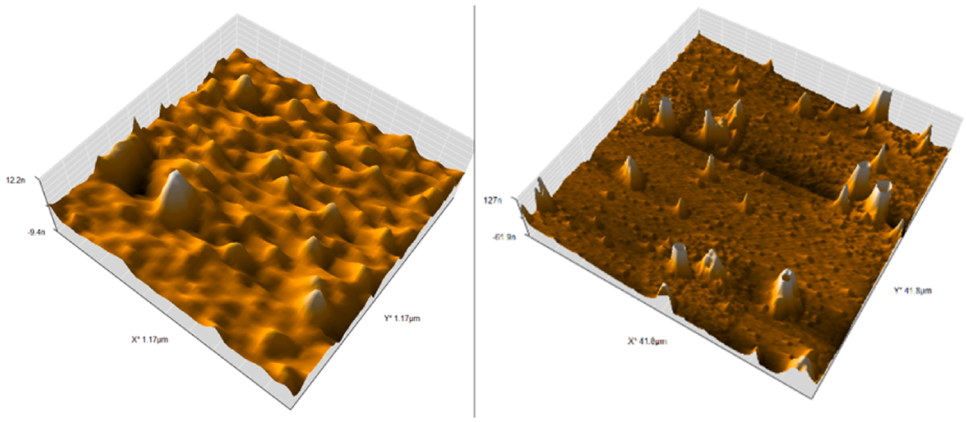

Fig. 15. 3D AFM images of γ-Al_2O_3–NPs powder.

Table 3
The diameter inhibition zone in (mm) units for samples (C_1–C_4) γ-Al_2O_3–NPs powder.

Microorganism	2 mg/mL (C1)	1 mg/mL (C2)	0.5 mg/mL (C3)	0.25 mg/mL (C4)
S. aureus	18	22	20	24
E. coli	20	22	25	27
C. albicans	20	22	21	25

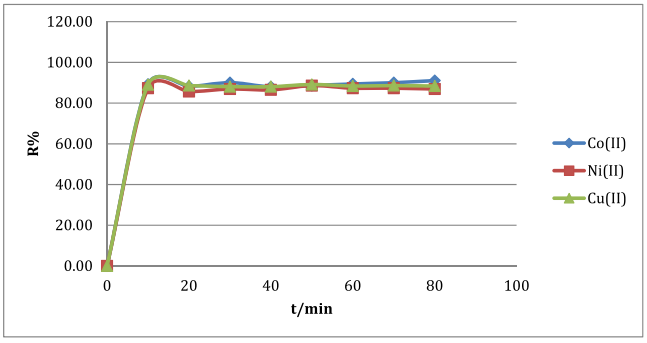

Fig. 16. Explain the efficiency of the removal of metal ions (Co, Ni, and Cu) by γ-Al_2O_3–NPs powder.

Within 10 min, equilibrium was reached in the adsorption process. After 10 min to 80 min, there was no discernible difference in metal ion elimination. The removal amount was enhanced by γ-Al_2O_3–NPs because in the first phase of adsorption, many potential sites are unfilled, and with the continuation of time, after the potential sites become saturated [41–43].

4. Conclusion

γ-Al_2O_3–NPs were synthesized by the green method using an aqueous extract of Boswellia carterii with a particle size of 17.5 nm. γ-Al_2O_3–NPs have a uniform size with plate–like and distribution. The antibacterial effect of Al_2O_3–NPs is generally sustained at concentrations ranging from 2 mg/mL to 0.25 mg/mL. This effect is attributed to the adsorption of these nanoparticles onto the bacterial surface and the formation of Al^{3+}, which promotes the generation of reactive oxygen species (ROS) that oxidize bacterial cells, resulting in cell death. The reported Al_2O_3–NPs on *Candida albicans* showed growth delay in it as well. This study focused on the removal of bivalent metal cation ions (Co, Ni, Cu) due to the unique features, such as active site, stability, and homogeneous large surface area. According to the high antibacterial activity and excellent ability to remove cations from aqueous solution, the prepared Al_2O_3–NPs can be considered as potent saviors against antibacterial activity and excellent adsorbents. We recommended in future used another plant of resin gums, such as Commiphora Myrrh Resin or Acacia Senegal, for future green synthesis and made a comparative study with Boswellia Carterii resin, and also studied the pharmaceutical and medical applications, focusing on potential drug delivery systems for these plants of resin gums.

Funding

This work was not financially supported by any institution.

CRediT authorship contribution statement

Waleed Khalid Mahdi: Writing – review & editing, Writing – original draft, Visualization, Validation, Supervision, Software, Resources, Project administration, Methodology, Investigation, Funding acquisition, Formal analysis, Data curation. **Aqeel Oudah Flayyh:** Methodology. **Falih Hassan Musa:** Writing – review & editing, Supervision. **Ahmed Saleem Otaiwi:** Writing – review & editing.

Declaration of competing interest

The authors declare that they have no known competing financial interests or personal relationships that could have appeared to influence the work reported in this paper.

Acknowledgements

Best grateful to all authors who supported and contributed to this work from the University of Baghdad College of Education of Pure Science (Ibn–Al–Haitham).

Data availability

The data that has been used is confidential.

References

[1] M.M. Abady, D.M. Mohammed, T.N. Soliman, R.A. Shalaby, F.A. Sakr, Sustainable synthesis of nanomaterials using different renewable sources, Bull. Natl. Res. Cent. 49 (1) (2025) 24, https://doi.org/10.1186/s42269-025-01316-4.
[2] A.I. Osman et al., "Synthesis of green nanoparticles for energy, biomedical, environmental, agricultural, and food applications: a review," 2024. doi: 10.1007/s10311-023-01682-3.
[3] L. Motiei, D. Margulies, Molecules that generate fingerprints: a new class of fluorescent sensors for chemical biology, medical diagnosis, and cryptography, Acc. Chem. Res. 56 (13) (2023), https://doi.org/10.1021/acs.accounts.3c00162.
[4] C. ZAFER, Nanotechnology, society and national security, Güven. Bilim. Derg. 10 (1) (2021), https://doi.org/10.28956/gbd.845173.
[5] Z. Alhalili, "Metal oxides nanoparticles: general structural description, chemical, physical, and biological synthesis methods, role in pesticides and heavy Metal removal through wastewater treatment," 2023. doi: 10.3390/molecules28073086.
[6] J.A. Saimon, et al., Synthesis and characterization of Al2O3 nanoparticles using PLAL with different Nd:YAG laser fluences for photodetectors, Plasmonics. 20 (1) (2025) 387–397, https://doi.org/10.1007/s11468-024-02288-3.
[7] I.L. Ikhioya, A.C. Nkele, Green synthesis and characterization of aluminum oxide nanoparticle using neem leaf extract (Azadirachta Indica), Hybrid. Adv. 5 (2024), https://doi.org/10.1016/j.hybadv.2024.100141.
[8] A.K. Saleh, A.S. Shaban, M.A. Diab, D. Debarnot, A.S. Elzaref, Green synthesis and characterization of aluminum oxide nanoparticles using Phoenix dactylifera seed extract along with antimicrobial activity, phytotoxicity, and cytological effects on Vicia faba seeds, BioMass Convers. Biorefin. (2023), https://doi.org/10.1007/s13399-023-04800-x.
[9] Y.E. Hassen, G. Gedda, A.H. Assen, D.M. Kabtamu, W.M. Girma, Dodonaea angustifolia extract-assisted green synthesis of the Cu2O/Al2O3 nanocomposite for adsorption of Cd(II) from water, ACS. Omega 8 (19) (May 2023) 17209–17219, https://doi.org/10.1021/acsomega.3c01609.
[10] M. Todera¸s, F.S. Aljohani, M. El-Khatib, Impact of electrical current on cluster nucleation production: phase, structure, and nanosize for Al2O3, J. Cryst. Growth 625 (2024) 127437, https://doi.org/10.1016/j.jcrysgro.2023.127437.
[11] S. Ghotekar, Plant extract mediated biosynthesis of Al2O3 nanoparticles- a review on plant parts involved, characterization and applications, Nanochemistry Res. 4 (2) (2019) 163–169, https://doi.org/10.22036/ncr.2019.02.008.
[12] L. Natrayan, Y.S. Rao, P.R. Prasad, K. Bhaskar, P.P. Patil, D.B. Abdeta, [Retracted] Biosynthesis-based Al2O3 nanofiller from Cymbopogon citratus leaf/Jute/Hemp/epoxy-based hybrid composites with superior mechanical properties, Bioinorg. Chem. Appl. 2023 (1) (Jan. 2023) 9299658, https://doi.org/10.1155/2023/9299658.
[13] S.V. Gudkov, D.E. Burmistrov, V.V. Smirnova, A.A. Semenova, and A.B. Lisitsyn, "A mini review of antibacterial properties of Al2O3 nanoparticles," 2022. doi: 10.3390/nano12152635.
[14] A.R.Z. Almotairy, A.M. Amer, H. El-Kady, B.H. Elwakil, M. El-Khatib, A. M. Eldrieny, Nanostructured γ-Al2O3 synthesis using an arc discharge method and its application as an antibacterial agent against XDR bacteria, Inorg. (Basel) 11 (1) (2023), https://doi.org/10.3390/inorganics11010042.
[15] W.K. Mahdi, A.O. Flayyih, F.H. Musa, Green synthesis, characterization, and applications of aluminum oxide nanoparticles using aqueous extract of clove, J. Kim. Val. 10 (2) (Nov. 2024) 277–289, https://doi.org/10.15408/jkv.v10i2.40403.
[16] W.K. Mahdi, A.O. Flayyih, F.H. Musa, Biosynthesis, characterization, and applications of aluminum oxide nanoparticles using aqueous extract of Cinnamon, AIP. Conf. Proc. 3219 (1) (Nov. 2024) 050006, https://doi.org/10.1063/5.0236391.
[17] K.B. Kusuma, et al., Photocatalytic and electrochemical sensor for direct detection of paracetamol comprising γ-aluminium oxide nanoparticles synthesized via sonochemical route, Sens. Int. 1 (2020), https://doi.org/10.1016/j.sintl.2020.100039.

[18] A.P. Kumar, D. Bilehal, A. Tadesse, D. Kumar, Photocatalytic degradation of organic dyes: Pd-γ-Al2O3 and PdO-γ-Al2O3 as potential photocatalysts, RSC. Adv. 11 (11) (2021) 6396–6406, https://doi.org/10.1039/D0RA10290C.
[19] P. Zemek, J. Van Gompel, and S. Plowman, "Ppm-level HCl measurements from cement kilns and waste incinerators by FTIR spectroscopy," MIDAC Corporation. Available online: http://www.midac.com/files/AP-212.pdf (accessed on 22 November 2022), 2012.
[20] Z. Gholizadeh, M. Aliannezhadi, M. Ghominejad, F.S. Tehrani, High specific surface area γ-Al2O3 nanoparticles synthesized by facile and low-cost co-precipitation method, Sci. Rep. 13 (1) (Apr. 2023) 6131, https://doi.org/10.1038/s41598-023-33266-0.
[21] E.O. Filatova, A.S. Konashuk, Interpretation of the changing the band gap of Al 2 O 3 depending on its crystalline form: connection with different local symmetries, J. Phys. Chem. C 119 (35) (Sep. 2015) 20755–20761, https://doi.org/10.1021/acs.jpcc.5b06843.
[22] A.F. Alamouti, M. Nadafan, Z. Dehghani, M.H.M. Ara, A.V. Noghreiyan, Structural and optical coefficients investigation of γ-Al2O3 nanoparticles using Kramers-Kronig relations and Z–scan technique, J. Asian Ceram. Soc. 9 (1) (Jan. 2021) 366–373, https://doi.org/10.1080/21870764.2020.1869881.
[23] S. Ghosh, P. Bose, S. Basak, M.K. Naskar, Solvothermal-assisted evaporation-induced self-assembly process for significant improvement in the textural properties of γ-Al 2 O 3 , and study dye adsorption efficiency, J. Asian Ceram. Soc. 3 (2) (Jun. 2015) 198–205, https://doi.org/10.1016/j.jascer.2015.02.005.
[24] T. Sabah, K.H. Jawad, N. Al-attar, Synthesis and biomedical activity of aluminium oxide nanoparticles by laser ablation technique, Res J Pharm. Technol. (Mar. 2023) 1267–1273, https://doi.org/10.52711/0974-360X.2023.00209.
[25] M. Farahmandjou, N. Golabiyan, Synthesis and characterisation of Al2O3 nanoparticles as catalyst prepared by polymer co-precipitation method, Mater. Eng. Res. 1 (2) (2019) 40–44, https://doi.org/10.25082/MER.2019.02.002.
[26] K. Parveen, U. Rafique, M.Javed Akhtar, M. Ashokkumar, Sonochemical synthesis of aluminium and aluminium hybrids for remediation of toxic metals, Ultrason. Sonochem. 70 (Jan. 2021) 105299, https://doi.org/10.1016/j.ultsonch.2020.105299.
[27] K. Djebaili, Z. Mekhalif, A. Boumaza, A. Djelloul, XPS, FTIR, EDX, and XRD analysis of Al 2 O 3 scales grown on PM2000 alloy, J. Spectrosc. 2015 (2015) 1–16, https://doi.org/10.1155/2015/868109.
[28] M. Cascione, V. De Matteis, F. Persano, S. Leporatti, AFM characterization of Halloysite Clay nanocomposites' Superficial properties: current State-of-the-art and perspectives, Mater. (Basel) 15 (10) (May 2022) 3441, https://doi.org/10.3390/ma15103441.
[29] D. Hill, A.R. Barron, S. Alexander, Controlling the wettability of plastic by thermally embedding coated aluminium oxide nanoparticles into the surface, J. Colloid. Interface Sci. 567 (May 2020) 45–53, https://doi.org/10.1016/j.jcis.2020.01.116.
[30] U. Utari, K. Kusumandari, B. Purnama, M. Mudasir, K. Abraha, Surface morphology of Fe(III)-porphyrin thin layers as characterized by atomic force microscopy, Indones. J. Chem. 16 (3) (Mar. 2018) 233, https://doi.org/10.22146/ijc.21136.
[31] M. Ranjbar, G. Dehghan Noudeh, M.-A. Hashemipour, I. Mohamadzadeh, A systematic study and effect of PLA/Al 2 O 3 nanoscaffolds as dental resins: mechanochemical properties, Artif. Cells Nanomed. Biotechnol. 47 (1) (Dec. 2019) 201–209, https://doi.org/10.1080/21691401.2018.1548472.
[32] A.I.S. Luis, E.V.R. Campos, J.L. de Oliveira, L.F. Fraceto, Trends in aquaculture sciences: from now to use of nanotechnology for disease control, Rev. Aquac. 11 (1) (Feb. 2019) 119–132, https://doi.org/10.1111/raq.12229.
[33] C. Adlhart, et al., Surface modifications for antimicrobial effects in the healthcare setting: a critical overview, J. Hosp. Infect. 99 (3) (2018) 239–249, https://doi.org/10.1016/j.jhin.2018.01.018.
[34] J.Y. Al-Humaidi, M. Hagar, B.A. Bakr, B.H. Elwakil, E.A. Moneer, M. El-Khatib, Decorative multi-walled carbon nanotubes by ZnO: synthesis, characterization, and potent anti-toxoplasmosis activity, Met. (Basel) 12 (8) (2022), https://doi.org/10.3390/met12081246.
[35] F.S. Aljohani, et al., Water treatment from MB using Zn-Ag MWCNT synthesized by double arc discharge, Mater. (Basel) 14 (23) (2021) 7205.
[36] A. Jawad, Q. Thewaini, S. Al-Musawi, Cytotoxicity effect and antibacterial activity of Al2O3 nanoparticles activity against Streptococcus Pyogenes and Proteus Vulgaris, J. Appl. Sci. Nanotechnol. 1 (3) (2021), https://doi.org/10.53293/jasn.2021.3944.1061.
[37] W.H. Organization, "WHO bacterial priority pathogens list, 2024: bacterial pathogens of public health importance, to guide research, development and strategies to prevent and control antimicrobial resistance,", World Health Organization, Geneva, 2024. Accessed: Aug. 15, 2025. [Online]. Available, https://books.google.iq/books?hl=en&lr=&id=UjAJEQAAQBAJ&oi=fnd&pg=PR6&ots=Ed4OFz4Pbl&sig=Y4KfMHFmaMAbKTIGKDn09AxBoGo&redir_esc=y#v=onepage&q&f=false.
[38] T.E. Oladimeji, M. Oyedemi, M.E. Emetere, O. Agboola, J.B. Adeoye, O. A. Odunlami, Review on the impact of heavy metals from industrial wastewater effluent and removal technologies, Heliyon. 10 (23) (Dec. 2024), https://doi.org/10.1016/j.heliyon.2024.e40370.
[39] Md.C. Sheikh, et al., Toxic cadmium(II) monitoring and removal from aqueous solution using ligand-based facial composite adsorbent, J. Mol. Liq. 389 (2023) 122854, https://doi.org/10.1016/j.molliq.2023.122854.
[40] R.M. Waliullah, et al., Optimization of toxic dye removal from contaminated water using chitosan-grafted novel nanocomposite adsorbent, J. Mol. Liq. 388 (2023) 122763, https://doi.org/10.1016/j.molliq.2023.122763.
[41] A.O. Flayyih, W.K. Mahdi, Y.I.M. Abu Zaid, F.H. Musa, Biosynthesis, characterization, and applications of bismuth oxide nanoparticles using aqueous extract of beta Vulgaris, Chem. Methodol. 6 (8) (Aug. 2022) 620–628, https://doi.org/10.22034/chemm.2022.342124.1522.
[42] Z. Bonyadi, Z. Fouladi, A. Robatjazi, M.Zahmatkesh Anbarani, Reactive red-141 removal from synthetic solutions by γ-Al2O3 nanoparticles: process modeling, kinetic, and isotherm studies, Appl. Water. Sci. 13 (2) (2023), https://doi.org/10.1007/s13201-022-01854-6.
[43] M.E. Awual, et al., Ligand imprinted composite adsorbent for effective Ni(II) ion monitoring and removal from contaminated water, J. Ind. Eng. Chem. 131 (2024) 585–592, https://doi.org/10.1016/j.jiec.2023.10.062.